

Long-range charge transport in single G-quadruplex DNA molecules

Gideon I. Livshits¹, Avigail Stern¹, Dvir Rotem¹, Natalia Borovok², Gennady Eidelstein², Agostino Migliore^{3,4}, Erika Penzo⁵, Shalom J. Wind⁵, Rosa Di Felice^{6,7}, Spiros S. Skourtis⁸, Juan Carlos Cuevas⁹, Leonid Gurevich¹⁰, Alexander B. Kotlyar^{2*} and Danny Porath^{1*}

DNA and DNA-based polymers are of interest in molecular electronics because of their versatile and programmable structures. However, transport measurements have produced a range of seemingly contradictory results due to differences in the measured molecules and experimental set-ups, and transporting significant current through individual DNA-based molecules remains a considerable challenge. Here, we report reproducible charge transport in guanine-quadruplex (G4) DNA molecules adsorbed on a mica substrate. Currents ranging from tens of picoamperes to more than 100 pA were measured in the G4-DNA over distances ranging from tens of nanometres to more than 100 nm. Our experimental results, combined with theoretical modelling, suggest that transport occurs via a thermally activated long-range hopping between multi-tetrad segments of DNA. These results could re-ignite interest in DNA-based wires and devices, and in the use of such systems in the development of programmable circuits.

Solid-state molecular electronics—the incorporation of molecules, as functional elements, into solid-state devices¹—is one approach to the miniaturization of memory storage and electronic devices using molecules². For such purposes, double-stranded (ds) DNA has been considered a natural electrical conduit^{3,4} or template⁵, primarily because of its molecular recognition and self-assembly properties⁶. Theoretical models⁷ suggest it could be used as a conductive wire, with sufficient delocalization for the transport of charge along the molecule. This naive view, however, does not take into account the deleterious effect of the surroundings on this soft biomolecule^{8,9}. In particular, in spite of some promising results (which have not been reproduced consistently), it is well established that long dsDNA adsorbed on a solid substrate shows no appreciable charge transport^{10–13}. Moreover, as the field has progressed, different experiments have been carried out on different DNA-based systems and in a variety of conditions, with seemingly contradictory or irreproducible results^{13–17}. In many cases, the results lack control over the measurement configuration, the number of molecules measured, and the nature of the contact to the molecules^{18–25}. Most importantly, the results have not provided sufficient evidence to determine specific charge transport mechanisms in the molecules.

G4-DNA as a molecular wire

To address these challenges we concentrated our studies on a more promising model system, guanine-quadruplex DNA (G4-DNA)^{26–30}. We synthesized a unique form of a relatively long DNA derivative (~250 nm), biotin-avidin (BA)-G4-DNA, as shown schematically in Fig. 1a. This is both stiffer than dsDNA and more likely to transport

charges over long distances because of its G-rich content^{7,31} and the additional charge transport pathways within the molecule^{28,32}. This derivative is composed of four strands of G nucleotides that run parallel to each other and form a braided quasi-one-dimensional structure, with the guanine tetrad (Fig. 1b) as a recurring unit. Each tetrad is composed of four G bases fortified by eight hydrogen bonds, furnishing it with greater rigidity than dsDNA base pairs²⁶. The overall structure is more robust and more likely to withstand the deformations induced by molecule–substrate interactions that may have a deleterious effect on electrical transport through the molecules^{8,33}. Electrostatic force microscopy studies show that G4-DNA^{26,30} yields a clear polarizability signal on a mica surface^{26,27,29}, while native dsDNA has no discernible signal^{29,34,35}, suggesting that G4-DNA may be capable of transporting electrical current²⁷.

Motivated by these results, we performed electrical transport measurements on BA-G4-DNA. A gold electrode was evaporated using stencil lithography on top of individual DNA molecules that had been pre-adsorbed onto a flat mica surface (Fig. 1c). In contrast to the standard lithography processes used to measure carbon nanotubes and other crystalline wires and nanorods, the molecules in this study were not subjected to chemicals, thus avoiding a central source of damage and contamination to the soft biomolecules. Our methodology produces very sharp and well-defined electrode edges (Fig. 1c), overcoming the indeterminate blurring effects³⁶ that may limit or interfere with the native transport properties of the molecules (for more examples see Supplementary Fig. 1). Metal clusters are found to impinge on the coated part of any individual molecule, while its free part appears morphologically intact (Supplementary Fig. 2).

¹Institute of Chemistry and The Center for Nanoscience and Nanotechnology, The Hebrew University of Jerusalem, Edmond J. Safra Campus, Jerusalem 91904, Israel, ²Department of Biochemistry and Molecular Biology, George S. Wise Faculty of Life Sciences and Center of Nanoscience and Nanotechnology, Tel Aviv University, Ramat Aviv 69978, Israel, ³Department of Chemistry, Duke University, Durham, North Carolina 27708, USA, ⁴School of Chemistry, Tel Aviv University, 69978 Tel Aviv, Israel, ⁵Department of Applied Physics and Applied Mathematics, 200 Mudd Building, 500 West 120th Street, Columbia University, New York 10027, USA, ⁶Department of Physics and Astronomy, University of Southern California, Los Angeles, California 90089, USA, ⁷Center S3, CNR Institute of Nanoscience, Via Campi 213/A, 41125 Modena, Italy, ⁸Department of Physics, University of Cyprus, Nicosia 1678, Cyprus, ⁹Departamento de Física Teórica de la Materia Condensada and Condensed Matter Physics Center (IFIMAC), Universidad Autónoma de Madrid, E-28049 Madrid, Spain, ¹⁰Department of Physics and Nanotechnology, Aalborg University, Skjernvej 4A, DK-9220 Aalborg, Denmark.

*e-mail: s2shak@post.tau.ac.il; danny.porath@mail.huji.ac.il

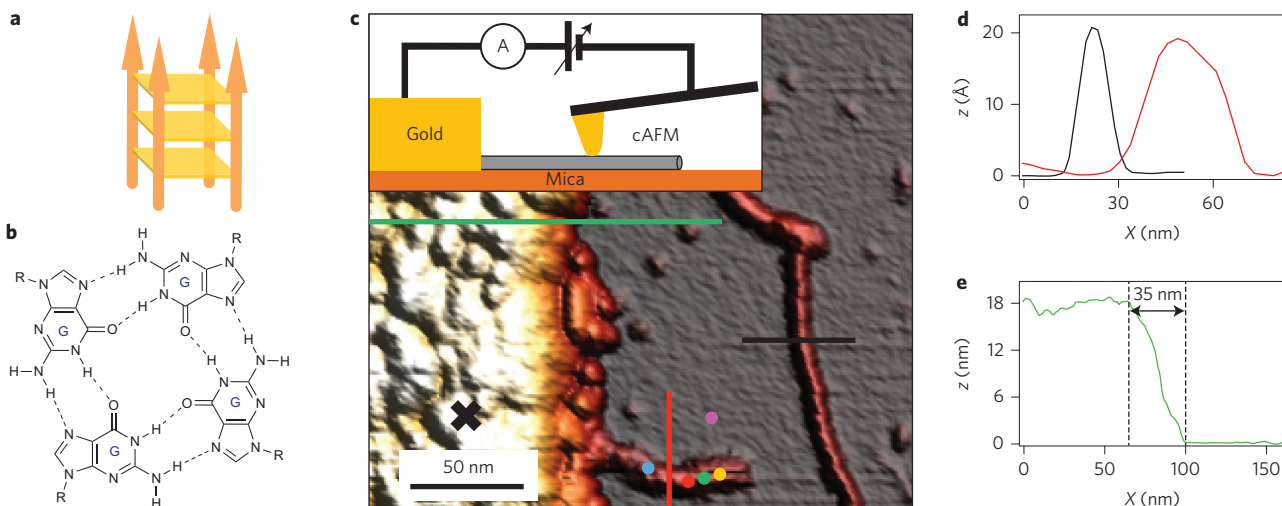


Figure 1 | Measurement set-up and sample image. **a**, BA-G4-DNA scheme showing an oriented ordered stack of tetrads. **b**, A single G4-DNA tetrad. **c**, AFM image showing a typical measurement scenario: a gold electrode with a sharp edge is on the left and molecules are clearly visible on the mica to the right; one molecule (at the bottom) is protruding from under the edge of the metal electrode. Inset: Schematic representation of the measurement set-up. **d**, Cross-sections of the free (black) and connected (red) molecules at the locations indicated by black and red lines in **c**, with a height typical of single BA-G4-DNA²⁶ (~2 nm). **e**, Profile across the electrode and mica, revealing a very clean and sharp termination of the electrode. The measured slope, which is 35 nm across, is a result of tip dilation. SEM imaging (as in Supplementary Fig. 1g) shows sharper termination.

The current–voltage (*I*–*V*) characteristics of BA-G4-DNA are presented in Fig. 2. In a typical experiment, a molecule was located by atomic force microscopy (AFM) imaging using a metallized tip. Subsequently, the tip was brought into contact with the molecule, and the current through the molecule was measured in response to bias voltage ramps up to ± 5 V. This procedure was repeated at different tip positions along the molecule. The measurement on each molecule started at its farthest free end in order to minimize any possible damage that could affect subsequent measurements. Forward and backward *I*–*V* characteristics at each point were reproducible, displaying no significant hysteresis for distances larger than 30 nm from the electrode edge. Figure 2a presents *I*–*V* curves measured at the positions marked by correspondingly coloured dots on the molecule in Fig. 1c. Measurements on the mica substrate surrounding the molecule indicated no observable current (Fig. 2a, left inset), while measurements on the gold electrode showed ohmic behaviour limited by a series resistor in the measurement set-up (Fig. 2a, right inset). Measurements that were taken close to the electrode showed currents of over 100 nA at 5 V (Supplementary Fig. 3), which may have originated from non-molecular processes, possibly as a result of field emission or partial contact between the tip edge and the evaporated electrode. Some of the molecules were scanned before and after the electrical measurements to check for drift or possible damage to the molecule. In some cases, images of the sample were taken and electrical measurements on the substrate were performed between successive electrical measurements on the molecule. In addition, electrical transport was re-measured several times at some positions on the molecule (Supplementary Fig. 4). Overall, electrical transport measurements were performed on 15 single BA-G4-DNA molecules, resulting in *I*–*V* curves similar to those shown in Fig. 2a on most samples (see Supplementary Information for more examples). Ten of the fifteen molecules showed clear and similar charge transport characteristics. Figure 2b shows the current values at 5 V measured at different positions along three molecules. These data demonstrate the relatively high currents that BA-G4-DNA molecules attached to a hard substrate can reproducibly transport. Several consecutive measurements in the same positions produced similar *I*–*V* characteristics (for more details see Supplementary Fig. 4). A collection of *I*–*V* curves from

measurements on many molecules at different positions along the molecules demonstrates the general reproducibility of the results (Fig. 2c). These measurements indicate a lower bound on the charge transport through G4-DNA.

The precise values of the current varied for different molecules at the same bias voltage, but several features stood out: (1) asymmetry between the current profiles at negative and positive bias voltages, with higher current at positive bias; (2) negligible current (below system noise, 2 pA) below ± 3 –4 V, followed by a rapid rise in the current; (3) weak and non-trivial dependence of the *I*–*V* data, especially the current rise, on the distance between the measured point and the border of the electrode (Figs 2a,c, 4c; Supplementary Figs 4a and 6).

To test the reliability of our results and the consistency of the experimental set-up, control measurements were performed on dsDNA (Fig. 3a–c), on single-walled carbon nanotubes (SWCNTs) (Fig. 3d–f) and on mica (left inset in Fig. 2a and Supplementary Fig. 3c–d), using procedures similar to those described above. In all the measurements on dsDNA, no current was observed up to ± 5 V (Fig. 3c; Supplementary Fig. 4c) for similar distances. This observation is consistent with previous measurements on dsDNA deposited on a hard substrate^{10–12}. It also indicates that the measured currents originate from intramolecular processes and are not related to extraneous effects induced by the surroundings, such as humidity or ionic conduction. Figure 3d presents an AFM image of a typical sample in which SWCNTs are deposited on mica; one of them is protruding under the evaporated electrode. *I*–*V* measurements on many such SWCNT segments revealed that most were well connected to the electrodes, displaying a nominally ohmic dependence (limited by the series protection resistor; Fig. 3f), which is characteristic of highly conductive SWCNTs^{37,38}.

Hopping transport model

Our results establish that BA-G4-DNA deposited on a hard substrate can transport significant current over a relatively long distance compared to other non-crystalline polymers. The measured length dependence paves the way for addressing the physical mechanism that enables long-range charge transport in a DNA-based molecule deposited on a surface. First-principles calculations have suggested

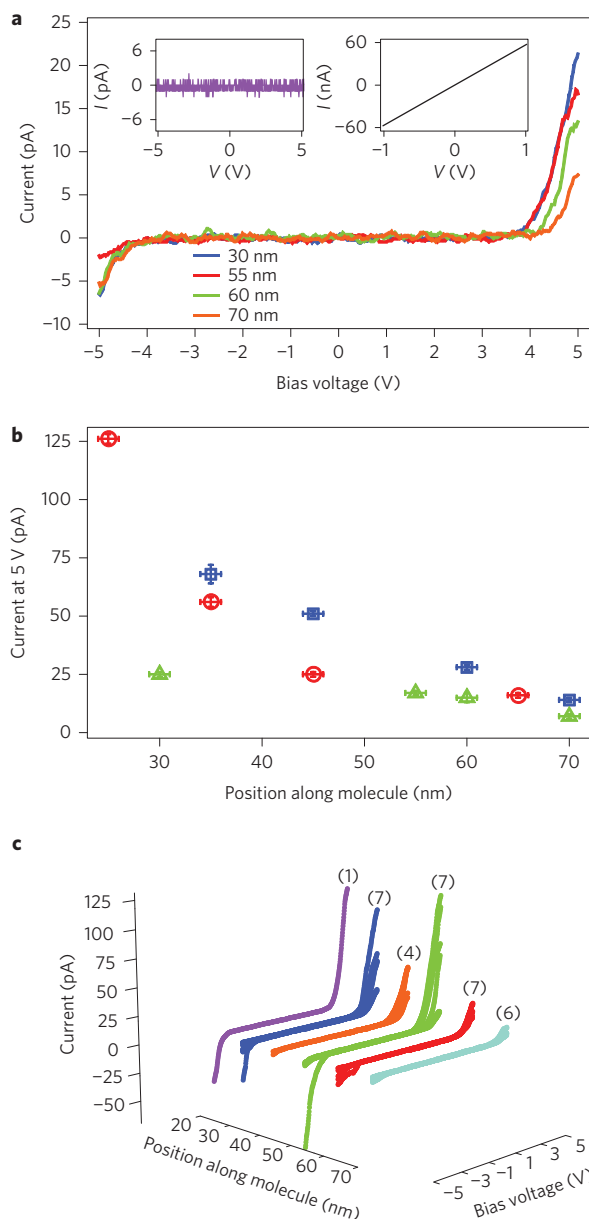


Figure 2 | I - V characteristics of BA-G4-DNA. **a**, I - V measurements taken at the positions indicated by coloured dots on the molecule shown in Fig. 1c. Left inset: I - V measurements on bare mica next to the molecule (magenta dot in Fig. 1c), showing noise-level currents. Right inset: I - V measurements on the gold electrode (black cross in Fig. 1c). **b**, Distance dependence of the current measured at a bias of 5 V for three different molecules (plotted in different colours). The error in tip position is determined from the experimental conditions (for example, stability of the scan). See Supplementary Section 1 for details. The error in the current is determined by fluctuations in the current and the noise associated with the gap. **c**, A collection of I - V curves measured on 10 different molecules. The current rises sharply at 3–4 V. The characteristics are grouped into 10 nm sections and the number of curves is given in parentheses. For more examples of measurements on the molecules see Supplementary Sections 1 and 2.

that G4-DNA molecules behave as wide-bandgap semiconductors with rather narrow (though wider than dsDNA) valence and conduction bands³¹. Thus, it is very likely that the charge transport found in our experiments is incoherent³².

To address this issue, we consider the simple hopping model sketched in Fig. 4a,b, which was inspired by recent publications^{39,40}.

Our basic assumption is that the charge transport along the molecule occurs via incoherent hopping through a series of N activation centres, which may be multi-tetrad blocks. We assume that a single state participates in the conduction in every activation centre. All activation centres are assumed identical, each with a single energy level, denoted δ (Fig. 4b). The voltage profile between the electrodes is described in terms of three parameters that account for the voltage drop at the left and right metal–molecule interfaces ($\alpha_{L,R}$) and across the molecule (α_M), such that $\alpha_L + \alpha_M + \alpha_R = 1$ (Fig. 4a,b). The key parameters in this model are the different bias-dependent rates describing electron transfer across the metal–molecule interfaces and between the activation centres inside the molecule. The forward and backward interfacial rates, $k_{L,R}^{\rightarrow,\leftarrow}(V)$, were calculated using the theory of electrochemical electron transfer⁴¹. Thus, the forward rate at the left interface, for instance, adopts the form

$$k_L^{\rightarrow}(V) = c_L \int_{-\infty}^{\infty} dx \frac{e^{-\left(x - \frac{\lambda + \delta + \alpha_L e V}{k_B T}\right)^2 \left(\frac{k_B T}{4\lambda}\right)}}{1 + e^x} \quad (1)$$

Here, c_L is a constant describing the strength of the metal–molecule coupling, λ is the interfacial reorganization energy associated with this electron transfer process, e is the electron charge, V is the voltage applied between the tip and the metal electrode, and T is the absolute temperature. The other interface rates have similar forms (Supplementary Section 2). For simplicity, we assume that all the forward and backward intramolecular rates are equal and are related via a detailed balance condition as follows: $k_f(V) = k e^{-\alpha_M e V / 2(N-1) k_B T}$ and $k_b(V) = k e^{\alpha_M e V / 2(N-1) k_B T}$, where k is the zero-bias intramolecular rate.

To determine the electrical current within this model, we first need to compute the stationary occupations in the different sites, P_i . These occupations are determined by solving the steady-state master equation³⁹:

$$\begin{aligned} \dot{P}_1 &= 0 = -(k_L^{\leftarrow} + k_f)P_1 + k_b P_2 + k_L^{\rightarrow} P_{L,R} \\ \dot{P}_2 &= 0 = -(k_b + k_f)P_2 + k_f P_1 + k_b P_3 \\ &\vdots \\ \dot{P}_N &= 0 = -(k_b + k_R^{\rightarrow})P_N + k_f P_{N-1} + k_R^{\leftarrow} P_{L,R} \end{aligned} \quad (2)$$

Here, the L and R indices correspond to the L and R effective electrode states³⁹. The system of equations (2) is supplemented by the normalization condition³⁹ $P_1 + P_2 + \dots + P_N + P_{L,R} = 1$, forming a system of $N+1$ algebraic linear equations. Once the different occupations have been determined, the corresponding electrical current (evaluated at the left interface) is given by

$$I(V) = -e(k_L^{\rightarrow} P_{L,R} - k_L^{\leftarrow} P_1) \quad (3)$$

For convenience, let us summarize the main parameters of this model, which will be adjusted to reproduce the experimental I - V characteristics: N (number of incoherent sites or activation centres), λ (interfacial reorganization energy), δ (the on-site molecular energy), k (zero-bias intramolecular transfer rate), $\alpha_{L,R}$ (the parameters describing the voltage drops at the metal–molecule interfaces) and $c_{L,R}$ (the pre-factors in the electrochemical transfer rates).

We used this model to fit the experimental I - V curves. For a given molecule, we began by adjusting the parameters to reproduce the results for the shortest measured distance from the edge of the electrode, after which all the parameters were fixed except for the strength of the coupling to the cAFM tip, the voltage drop at the tip–molecule interface and the number of activation centres.

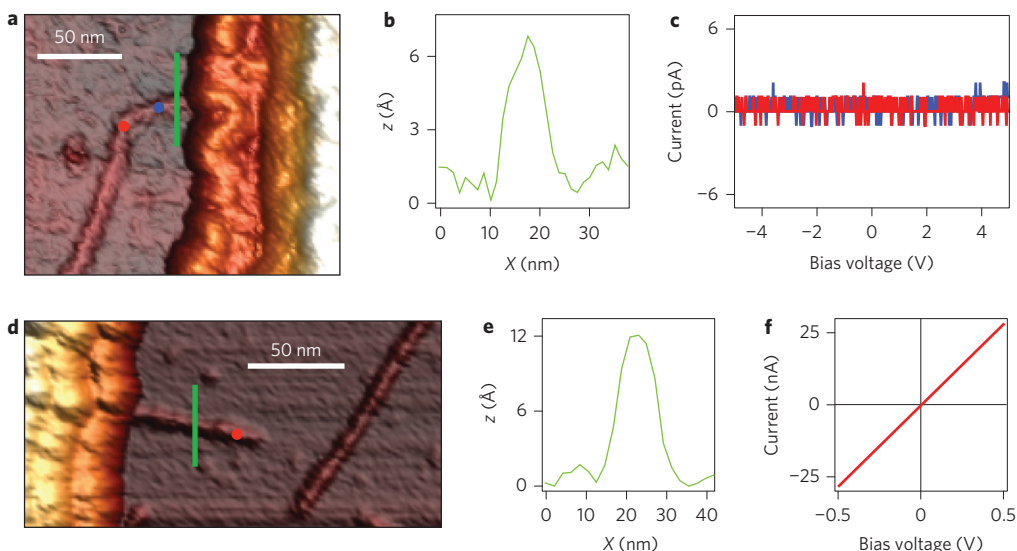


Figure 3 | Reference I - V measurements on dsDNA and SWCNT. **a**, AFM image of a micrometre-long dsDNA molecule adsorbed on mica and protruding from a gold electrode (right). **b**, Height profile across the molecule (green line in **a**), with a height typical of dsDNA. **c**, I - V measurements corresponding to the dots in **a** at a distance of 30 nm (blue) and 50 nm (red) from the electrode border. No current was observed in dsDNA for distances greater than 30 nm for bias voltages up to ± 8 V (Supplementary Fig. 4). **d**, AFM image of SWCNTs adsorbed on a mica substrate. One of the molecules is protruding from under an evaporated gold electrode (left). **e**, Height profile across the SWCNT (green line in **d**). **f**, Linear I - V curve measured 60 nm from the border (red dot in **d**). The slope yields the resistance of a current-limiting resistor ($17.7 \pm 0.1 \text{ M}\Omega$). More control measurements are shown in Supplementary Figs 3 and 4.

As demonstrated in Fig. 4c, we were able to consistently fit the experimental I - V curves using the same energy for the relevant bridge level, $\delta = 0.55$ eV, and the same value of the zero-bias intramolecular rate, $k \approx 1 \times 10^8 \text{ s}^{-1}$ (Table 1 presents a complete list of the values of the fit parameters). The fit is insensitive to variations of k within an order of magnitude (for a fixed N see Supplementary Fig. 6), due to the fact that transport is limited by the interfacial rates (see following discussion), whereas N is determined within ± 1 units (for details see Supplementary Fig. 6). The voltage drop at the right interface decreases with increasing effective length of the molecule (Supplementary Table 1), which is consistent with an increasing voltage drop across the molecule. All our experimental results were fitted with fixed parameters similar to those noted above, with a level of accuracy similar to that of Fig. 4c (as shown in Supplementary Section 2). From these results we find that the distance between hopping sites is of the order of 10–11 tetrads (~ 3.5 nm). This value, which correlates with the pitch of tetra-molecular G4-DNA on gold in scanning tunnelling microscopy (STM) measurements^{42,43}, gives the extent of electron delocalization along the quadruplex.

To assess the quality of the fit, and its correlation with the microscopic properties of the G4-DNA in our experiments, we calculated the effective electronic coupling between two adjacent tetrads (computed in the framework of hybrid density functional theory, DFT⁴⁴). This value, 0.26 eV, is larger than in results obtained with some semi-empirical electronic structure methods for G4-DNA that contained monovalent alkali ions and were thus characterized by larger values of the inter-tetrad stacking distance. Furthermore, it is consistent with an adiabatic hopping mechanism, borderline with band transport for reorganization energy values up to 1 eV (Supplementary Sections 3 and 4). Specifically, because the reorganization energy has never been computed for G4-DNA, we resort to values computed for related polymers (dsDNA) or to the model estimate. The model fit yields an interfacial reorganization energy of 0.5–0.6 eV, which corresponds to an intramolecular reorganization energy of at least 1.0 eV (ref. 45). Applying the latter value to Landau-Zener theory⁴⁵ (Supplementary Section 4) together with the effective electronic coupling for adjacent tetrads, we obtain an

inter-tetrad transfer rate of $\sim 1 \times 10^9 \text{ s}^{-1}$, consistent with the model fit of $k \approx 1 \times 10^8 \text{ s}^{-1}$ over ten tetrads. Thus, the DFT calculations help us to indirectly reduce the degrees of freedom of the model and strengthen the fits.

Conclusions

The scenario suggested by this model can be described as follows. Transport in the molecules is highly bias-dependent and is mainly limited by the interface rates, which are much smaller than k at high bias. Moreover, the model suggests the following explanation for the main features of the I - V curves. (1) The asymmetry in the I - V measurements is due to asymmetry in the metal–molecule coupling; that is, the contact at the evaporated electrode is much better and more reproducible than the tip–molecule contact, which probably changes from point to point, and in turn leads to an asymmetric voltage profile. (2) The strong current suppression below a threshold voltage is due to both the existence of an intrinsic gap in the molecule and the finite reorganization energy associated with charge injection in the molecule. (3) The rapid rise in the current above threshold reflects the bias dependence of the injection rates, because the charge injection is the rate-limiting process at high bias. (4) The threshold depends slightly on the measured length of the molecule, because the voltage profile inside the molecule and, in turn, the energy of the relevant molecular levels, depends on this length. (5) The unusual length dependence of the current, which does not fit into any of the standard length dependences (that is, it is neither exponential nor a simple power law), stems from the fact that the exact voltage profile also depends on the measured length of the molecule and this profile affects both the intramolecular rate and the metal–molecule interface rates.

It is worth stressing that although this hopping model is able to reproduce all the salient features of our experimental I - V curves, it has obvious limitations. For instance, it does not provide information about the nature of the hopping centres or about the role of the interaction between the substrate and the molecule. In this sense, it would be highly desirable to shed more light on the transport mechanism in our molecular junctions based on a more

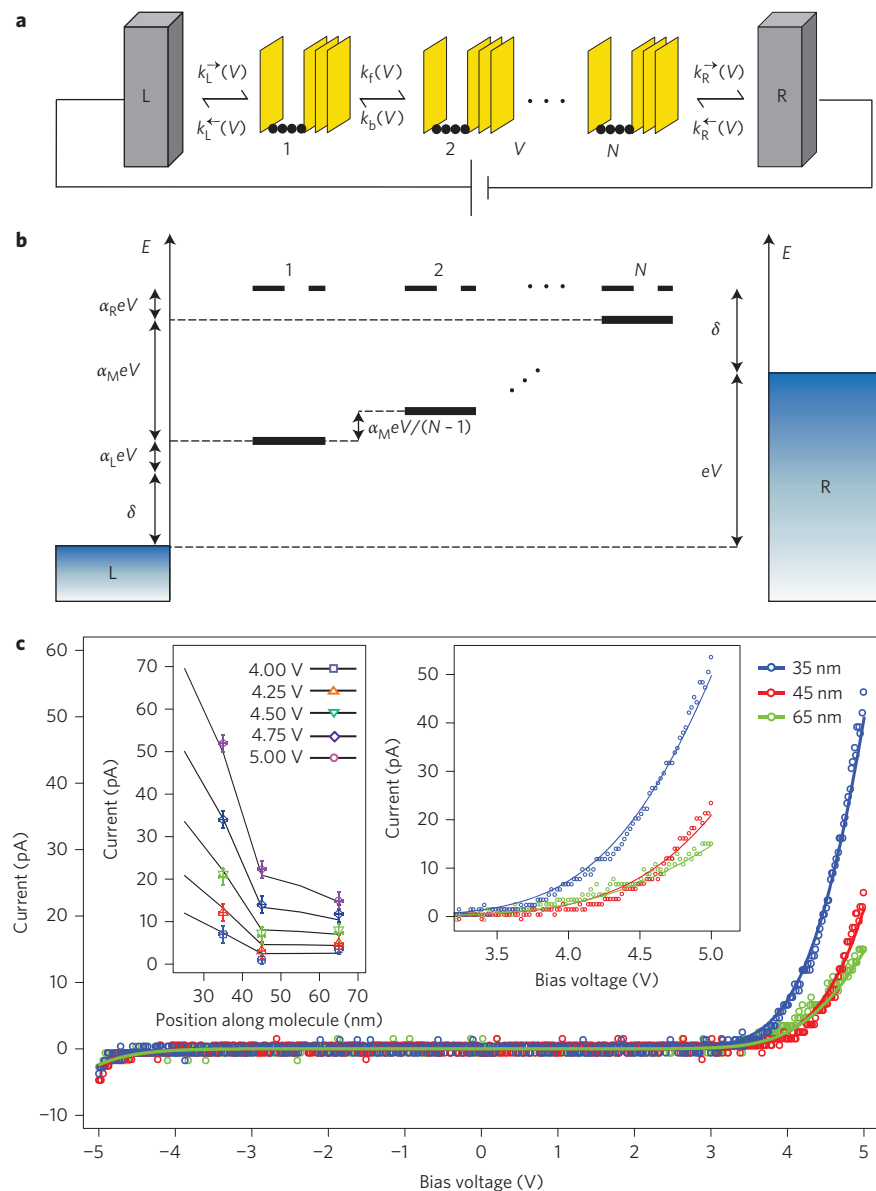


Figure 4 | The hopping transport model. **a**, Scheme of the one-dimensional hopping model, with incoherent hopping between adjacent sites, which represent multi-tetrad blocks. **b**, Energy diagram, including the voltage profile, used in the calculation of the current. **c**, Fit of the model (solid lines) to the experimental data (circles) on one representative molecule. Right inset: Enlargement of the current rise and its fit of the I - V measurements. Left inset: Length dependence of the current at different voltages. The data points correspond to the measured values, and the solid lines are model calculations. See Table 1 for fit parameters of the hopping transport model used to fit the curves in **c**.

Table 1 | Fit parameters of the hopping transport model used to compute the different curves in Fig. 4c.

Curve	N	λ (eV)	δ (eV)	k (10^8 s^{-1})	α_L	α_R	c_L (10^8 s^{-1})	c_R (10^8 s^{-1})
35 nm	10	0.6	0.55	1.0	0.135	0.200	2.0	1.0
45 nm	13	0.6	0.55	1.0	0.135	0.180	2.0	1.0
65 nm	19	0.6	0.55	1.0	0.135	0.183	2.0	1.0

For more examples of data and fitting to the data, see Supplementary Sections 2–4.

microscopic modelling. To facilitate this task, we present our experimental data in the Supplementary Information (including data files).

Over the past two decades, achievements in molecular electronics have mainly been related to monolayers, sensors and electrical transport through short molecules. Central challenges remained,

however, in transporting current in long polymer wires, in understanding the basic rules of this transport, and in implementing it in more complex electrical circuits. Our results represent a major step forward in this regard, providing the most reliable and controlled platform for such measurements in polymer wires that can transport significant current over long distances when deposited on a hard substrate, which is the more relevant configuration for solid-state devices. We also provide deep insight into the possible mechanism governing transport in these wires—thermally activated hopping between multi-tetrad segments. Our results pave a way towards the implementation of DNA-based programmable circuits for molecular electronics.

Methods

Experiments. BA-G4-DNA solution was prepared as described by Borovok and colleagues²⁶ with minor changes. dsDNA (pUC19) was obtained from Fermentas (part of Thermo Fisher Scientific). ssDNA-wrapped SWCNTs were prepared as

described by Zheng and co-authors⁴⁶. A volume of 20–40 μl of 1–2 nM BA-G4-DNA in 20 mM HEPES and 2 mM MgCl₂ was incubated on freshly cleaved mica for 15–60 min, washed with distilled water and dried with nitrogen gas, yielding a surface density of ~6–10 molecules μm^{-2} . Similar parameters were used for the deposition of dsDNA and SWCNTs. The samples were scanned by AFM (Nanotec Electronica S.L., dynamic mode) to verify surface coverage, then mounted under a stencil mask, directly placed on a sample and mask holder, and transferred to a thermal evaporator (modified Edwards E306). When base pressure reached $\sim 2 \times 10^{-6}$ torr, a cold trap was cooled to approximately -190 °C using liquid nitrogen. To overcome blurring effects, the mask was electrostatically clamped to the substrate, based on the principles described by Couderc and co-authors⁴⁷. The sample was cooled by a cooling agent flow. The substrate temperature dropped within 30 s to approximately -11 °C and then gradually to -25 °C. As soon as the temperature stabilized, slow evaporation began at $\sim 1 \text{ \AA min}^{-1}$ for 20 min. The evaporation rate was gradually increased by a factor of 2–4 until the end of the coating. A gold layer, 18–35 nm thick, was evaporated, typically within 60–90 min. The sample was transferred to a sample holder for electrical characterization in a second AFM system (AIST-NT, SmartSPM 1000, equipped with a cAFM module). *I*-*V* characteristics were measured using soft cantilevers (OMCL-RC800PSA, Olympus Optical Co.) with a nominal force constant of 0.3 N m⁻¹. The cantilevers were sputter-coated with \sim 30–40 nm of Au/Pd, which altered the nominal resonance frequency from 75–80 kHz to 50–60 kHz and tip radius from 15–20 nm to 30–50 nm (measured with a scanning electron microscope, SEM), respectively. For cAFM measurements, a molecule protruding from under the evaporated electrode was located in dynamic mode. The tip was then brought into contact at a desired position. Several force values were attempted before a clear current signal appeared. This value was used in all subsequent measurements on all samples. The images were analysed using Nanotec Electronica S.L WSxM imaging software⁴⁸.

Theory. DFT calculations were performed with NWChem software⁴⁹ using the Becke half-and-half functional and a variety of basis sets ranging from 6-311g* to 6-311++g**, as detailed in the Supplementary Information. The computed value of the electronic coupling between two adjacent guanine tetrads, determined according to a full-electron approach⁴⁴, was used to validate the fitting model. The geometry of stacked tetrads was extracted from the average structure of a 24-tetrad parallel G-quadruplex from a classical molecular dynamics simulation in explicit water with Li⁺ counterions⁵⁰, which occasionally (and not permanently) penetrate the channel. This geometry was not relaxed further by DFT. Only the structural elements that contribute to frontier orbitals (namely, the guanines)—and are consequently relevant to charge transfer rates—were included in DFT calculations. The details of the relation between the electronic coupling, the reorganization energy and the transfer rates, together with a discussion of transport regimes with a hopping mechanism, are provided in the Supplementary Information.

Received 4 March 2014; accepted 24 September 2014;
published online 26 October 2014

References

- Cuevas, J. C. & Scheer, E. *Molecular Electronics: An Introduction to Theory and Experiment* (World Scientific, 2010).
- Aradhya, S. V. & Venkataraman, L. Single-molecule junctions beyond electronic transport. *Nature Nanotech.* **8**, 399–410 (2013).
- Aviram, A. & Ratner, M. A. Molecular rectifiers. *Chem. Phys. Lett.* **29**, 277–283 (1974).
- Eley, D. D. & Spivey, D. I. Semiconductivity of organic substances. Part 9. Nucleic acid in the dry state. *Trans. Faraday Soc.* **58**, 411–415 (1962).
- Kumar, A., Hwang, J. H., Kumar, S. & Nam, J. M. Tuning and assembling metal nanostructures with DNA. *Chem. Commun.* **49**, 2597–2609 (2013).
- Seeman, N. C. DNA in a material world. *Nature* **421**, 427–431 (2003).
- Bixon, M. et al. Long-range charge hopping in DNA. *Proc. Natl Acad. Sci. USA* **96**, 11713–11716 (1999).
- Heim, T., Deremes, D. & Vuillaume, D. Conductivity of DNA probed by conducting-atomic force microscopy: effects of contact electrode, DNA structure, and surface interactions. *J. Appl. Phys.* **96**, 2927–2936 (2004).
- Gutierrez, R., Porath, D. & Cuniberti, G. in *Charge Transport in Disordered Solids with Applications in Electronics* (ed. Baranovski, S.) Ch. 9, 433–464 (Wiley, 2006).
- Braun, E., Eichen, Y., Sivan, U. & Ben-Yoseph, G. DNA-templated assembly and electrode attachment of a conducting silver wire. *Nature* **391**, 775–778 (1998).
- De Pablo, P. J. et al. Absence of dc-conductivity in lambda-DNA. *Phys. Rev. Lett.* **85**, 4992–4995 (2000).
- Storm, A. J., van Noort, J., de Vries, S. & Dekker, C. Insulating behavior for DNA molecules between nanoelectrodes at the 100 nm length scale. *Appl. Phys. Lett.* **79**, 3881–3883 (2001).
- Porath, D., Cuniberti, G. & Di Felice, R. Charge transport in DNA-based devices. *Top. Curr. Chem.* **237**, 183–227 (2004).
- Porath, D., Lapidot, N. & Gomez-Herrero, J. in *Introducing Molecular Electronics* (eds Cuniberti, G., Fagas, G. & Richter, K.) 411–444 (Springer, 2005).
- Astakhova, T. Y., Likhachev, V. N. & Vinogradov, G. A. Long-range charge transfer in biopolymers. *Russ. Chem. Rev.* **81**, 994–1010 (2012).
- Muren, N. B., Olmon, E. D. & Barton, J. K. Solution, surface, and single molecule platforms for the study of DNA-mediated charge transport. *Phys. Chem. Chem. Phys.* **14**, 13754–13771 (2012).
- Endres, R. G., Cox, D. L. & Singh, R. R. P. Colloquium: the quest for high-conductance DNA. *Rev. Mod. Phys.* **76**, 195–214 (2004).
- Fink, H. W. & Schonenberger, C. Electrical conduction through DNA molecules. *Nature* **398**, 407–410 (1999).
- Porath, D., Bezryadin, A., de Vries, S. & Dekker, C. Direct measurement of electrical transport through DNA molecules. *Nature* **403**, 635–638 (2000).
- Xu, B. Q., Zhang, P. M., Li, X. L. & Tao, N. J. Direct conductance measurement of single DNA molecules in aqueous solution. *Nano Lett.* **4**, 1105–1108 (2004).
- Cohen, H., Nogues, C., Naaman, R. & Porath, D. Direct measurement of electrical transport through single DNA molecules of complex sequence. *Proc. Natl. Acad. Sci. USA* **102**, 11589–11593 (2005).
- Guo, X. F., Gorodetsky, A. A., Hone, J., Barton, J. K. & Nuckolls, C. Conductivity of a single DNA duplex bridging a carbon nanotube gap. *Nature Nanotech.* **3**, 163–167 (2008).
- Watanebe, H., Manabe, C., Shigematsu, T., Shimotani, K. & Shimizu, M. Single molecule DNA device measured with triple-probe atomic force microscope. *Appl. Phys. Lett.* **79**, 2462–2464 (2001).
- Rakitin, A. et al. Metallic conduction through engineered DNA: DNA nanoelectronic building blocks. *Phys. Rev. Lett.* **86**, 3670–3673 (2001).
- Cai, L. T., Tabata, H. & Kawai, T. Self-assembled DNA networks and their electrical conductivity. *Appl. Phys. Lett.* **77**, 3105–3106 (2000).
- Borovok, N. et al. Assembling of G-strands into novel tetra-molecular parallel G4-DNA nanostructures using avidin/biotin recognition. *Nucleic Acids Res.* **36**, 5050–5060 (2008).
- Livshits, G. I., Ghabboun, J., Borovok, N., Kotlyar, A. & Porath, D. Comparative EFM of mono- and tetra-molecular G4-DNA. *Adv. Mater.* **26**, 4981–4985 (2014).
- Liu, S. P. et al. Direct measurement of electrical transport through G-quadruplex DNA with mechanically controllable break junction electrodes. *Angew. Chem. Int. Ed.* **49**, 3313–3316 (2010).
- Cohen, H. et al. Polarizability of G4-DNA observed by electrostatic force microscopy measurements. *Nano Lett.* **7**, 981–986 (2007).
- Kotlyar, A. B. et al. Long, monomolecular guanine-based nanowires. *Adv. Mater.* **17**, 1901–1904 (2005).
- Calzolari, A., Di Felice, R., Molinari, E. & Garbesi, A. G-quartet biomolecular nanowires. *Appl. Phys. Lett.* **80**, 3331–3333 (2002).
- Woiczikowski, P. B., Kubar, T., Gutierrez, R., Cuniberti, G. & Elstner, M. Structural stability versus conformational sampling in biomolecular systems: why is the charge transfer efficiency in G4-DNA better than in double-stranded DNA? *J. Chem. Phys.* **133**, 035103 (2010).
- Kasumov, A. Y., Klinov, D. V., Roche, P. E., Gueron, S. & Bouchiat, H. Thickness and low-temperature conductivity of DNA molecules. *Appl. Phys. Lett.* **84**, 1007–1009 (2004).
- Bockrath, M. et al. Scanned conductance microscopy of carbon nanotubes and lambda-DNA. *Nano Lett.* **2**, 187–190 (2002).
- Gomez-Navarro, C. et al. Contactless experiments on individual DNA molecules show no evidence for molecular wire behavior. *Proc. Natl Acad. Sci. USA* **99**, 8484–8487 (2002).
- Vazquez-Mena, O. et al. Analysis of the blurring in stencil lithography. *Nanotechnology* **20**, 415303 (2009).
- Bachtold, A. et al. Scanned probe microscopy of electronic transport in carbon nanotubes. *Phys. Rev. Lett.* **84**, 6082–6085 (2000).
- De Pablo, P. J. et al. Mechanical and electrical properties of nanosized contacts on single-walled carbon nanotubes. *Adv. Mater.* **12**, 573–576 (2000).
- Polizzetti, N. F., Skourtis, S. S. & Beratan, D. N. Physical constraints on charge transport through bacterial nanowires. *Faraday Discuss.* **155**, 43–62 (2012).
- Lehmann, J., Ingold, G. L. & Hanggi, P. Incoherent charge transport through molecular wires: interplay of Coulomb interaction and wire population. *Chem. Phys.* **281**, 199–209 (2002).
- Chidsey, C. E. D. Free-energy and temperature-dependence of electron-transfer at the metal–electrolyte interface. *Science* **251**, 919–922 (1991).
- Shapir, E. et al. High-resolution STM imaging of novel single G4-DNA molecules. *J. Phys. Chem. B* **112**, 9267–9269 (2008).
- Roger-Eitan, I. et al. High-resolution scanning tunneling microscopy imaging of biotin-avidin-G4-DNA molecules. *J. Phys. Chem. C* **117**, 22462–22465 (2013).
- Migliore, A. Full-electron calculation of effective electronic couplings and excitation energies of charge transfer states: application to hole transfer in DNA pi-stacks. *J. Chem. Phys.* **131**, 114113 (2009).
- Nitzan, A. *Chemical Dynamics in Condensed Phases* (Oxford Univ. Press, 2006).
- Zheng, M. et al. Structure-based carbon nanotube sorting by sequence-dependent DNA assembly. *Science* **302**, 1545–1548 (2003).
- Couderc, S., Blech, V. & Kim, B. New surface treatment and microscale/nanoscale surface patterning using electrostatically clamped stencil mask. *Jpn. J. Appl. Phys.* **48**, 095007 (2009).

48. Horcas, I. *et al.* WSXM: a software for scanning probe microscopy and a tool for nanotechnology. *Rev. Sci. Instrum.* **78**, 013705 (2007).
49. Valiev, M. *et al.* NWChem: a comprehensive and scalable open-source solution for large scale molecular simulations. *Comput. Phys. Commun.* **181**, 1477–1489 (2010).
50. Cavallari, M., Calzolari, A., Garbesi, A. & Di Felice, R. Stability and migration of metal ions in G4-wires by molecular dynamics simulations. *J. Phys. Chem. B* **110**, 26337–26348 (2006).

Acknowledgements

The authors thank E. Mastov, T. Dagan, J. Ghabboun, J. Gomez-Herrero, I. Lapides, D. Evplov, D. Park, V. Gutkin, I. Brodsky, E. Molinari, A. Garbesi, R. Rohs, D. N. Beratan, A. Nitzan and T. Milledge for technical support and discussions. *Ab initio* computations were performed using the Duke Shared Cluster Resource. This work was supported by the European Commission through grants ‘DNA-based nanowires’ (IST-2001-38951), ‘DNA-based nanodevices’ (FP6-029192) and FP7-ERC 226628, by the European Science Foundation COST MP0802, the Israel Science Foundation (1145/10 and 1589/14), Binational Science Foundation (BSF) grant 2006422, the Minerva Center for Bio-Hybrid complex systems, the Institute for Advanced Studies of the Hebrew University of Jerusalem, the Italian Institute of Technology project MOPROSURF, Fondazione Cassa di Risparmio di Modena, the Office of Naval Research (award no. N00014-09-1-1117) and the National

Science Foundation (grant CHE-1057953). D.P. thanks the Etta and Paul Schankerman Chair of Molecular Biomedicine.

Author contributions

D.P. and G.I.L. conceived and designed the reported research. G.I.L. prepared the samples and performed the CAFM experiments, assisted by A.S., D.R. and L.G. A.B.K., N.B. and G.E. designed and synthesized the G4-DNA molecules. S.J.W. and E.P. provided ssDNA-wrapped SWCNTs. J.C.C. and S.S.S. formulated the hopping model for the reported data, proposed by D.P. J.C.C. and G.I.L. fitted the data. J.C.C., S.S.S., A.M., R.D.F., G.I.L. and D.P. analysed the data. A.M. and R.D.F. conducted molecular dynamics simulations and DFT calculations for the G4-DNA structural and electrical properties. All authors discussed the results. G.I.L., J.C.C., R.D.F., S.S.S. and D.P. wrote the manuscript, assisted by all authors.

Additional information

Supplementary information is available in the [online version](#) of the paper. Reprints and permissions information is available online at www.nature.com/reprints. Correspondence and requests for materials should be addressed to A.B.K. and D.P.

Competing financial interests

The authors declare no competing financial interests.